PCCP

ARTICLE TYPE

Cite this: DOI: 00.0000/xxxxxxxxxx

The Reassigned Pseudo Wigner-Ville Transform in Electrochemical Noise Analysis

Ivana Jevremovic,* and Andreas Erbe

Received Date
Accepted Date

DOI: 00.0000/xxxxxxxxxx

Several different time-frequency transforms from signal processing were used to analyze electrochemical noise data to determine frequency components contained within the noise record and their time evolution. Bilinear time-frequency representations (TFR) based on the Wigner-Ville distribution (WVD) were compared with a special focus on the reassigned smoothed pseudo WVD (RSPWVD). Spectra obtained with WVD were compared with traditional linear time-frequency representations, such as short time Fourier transform and wavelet transform. Comparison to other TFRs showed that the RSPWVD suppressed artifacts, provided better resolution of the time-frequency analysis in both time and frequency domains, and improved the overall readability of a representation. The obtained spectra from RSPWVD were consistent with the results from DWT, but permitted a more comprehensive analysis of transients. Consequently, RSPWVD is suitable for electrochemical noise analysis. In the presence of Cl^-, RSPWVD showed that the passivity of Al was compromised, as evidenced by the presence of various current transients in the frequency range from 10^{-2} to 1 Hz.

1 Introduction

Electrochemical noise (EN) measurement is a noninvasive in situ electrochemical method that has the potential to deliver complimentary information about different electrochemical processes not available by other classical electrochemical methods. EN has been used for characterization and corrosion monitoring,[1,2] as a nondestructive diagnosis tool for fuel cells,[3–5] for batteries,[6,7] for the evaluation of catalyst performance,[8–10] and for characterization of electroplating processes.[11–13] In particular, in corrosion, EN should offer the intrinsic time and frequency scales that are observed in and relevant for the corrosion process.

EN data can be obtained in different ways as the fluctuations of potential and current under open circuit conditions, or under anodic or cathodic polarization of the working electrode.[14,15] EN data offers a lot of information about reaction mechanisms that is by no means straightforward, easy to classify and understand. Data can be analyzed in the time, frequency or time-frequency domain. Characterization in the time domain can be performed using sequence-independent methods such as moments, standard statistical parameters, skew, kurtosis, or root mean square.[16,17] On the other hand, for the presentation of the spectrum and to estimate the amplitudes of the different components in the analyzed signal, data is analyzed by application of fast Fourier transformation (FFT) or the maximum entropy method (MEM).[18,19] EN enables an identification of corrosion types occurring on the electrode surface, of corrosion mechanisms and of kinetics from the calculation of different parameters such as noise resistance, localization index, power spectral density (PSD) and spectral noise resistance, which can be compared with the magnitude of the electrochemical impedance at the same frequency.[20]

Time-frequency representations provide a powerful tool for the analysis of EN data. The aim of a joint time-frequency analysis is to directly represent the frequency content of the noise data while still keeping the time description parameter. In time-frequency analysis of EN data, different methods have been used, such as the short-time Fourier transform (STFT),[21,22] and the wavelet transform.[23,24] Recently, the Hilbert-Huang transform has been employed for the decomposition of individual transients into their instantaneous frequencies.[25,26] Corrosion processes are often non-stationary and nonlinear, and consequently characterized by a DC drift of the signal. The presence of a baseline trend in EN data can also be the result of a slow alteration of the system caused by changes in its chemical composition (e.g. solvation, species dissolution), small fluctuations in the temperature or increasing asymmetry between working electrodes. The problem is particularly complicated when dealing with low intensity signals. For instance, passive electrodes are polarizable and hence more susceptible to potential fluctuations.

Unless baseline wander is removed prior to further analysis, the low frequency drift will dominate the data and mask impor-

[a] Department of Materials Science and Engineering, NTNU, Norwegian University of Science and Technology, 7491 Trondheim, Norway;
* corresponding author, E-mail: ec-noise-analysis@the-passivists.org

tant information. The choice of the method is known as one of the most challenging problems in EN analysis.[27] Many procedures to remove drift have been presented so far, including linear trend removal,[28] polynomial fitting, digital filtering,[29] wavelet transform, empirical mode decomposition,[30] or employment of a discrete version of the Wiener-Khinchin theorem.[31] Nevertheless, selecting the ideal method to deal with the baseline problem and to distinguish the drift from the useful information remains open.

The purpose of this paper is to evaluate the suitability of a time-frequency decomposition based on the Wigner-Ville distribution (WVD) for the analysis of EN signals by comparing it to linear time-frequency methods for spectral estimation of EN. WVD is the Fourier transform of instantaneous autocorrelation function of a signal and was first introduced by Wigner in quantum mechanics and was reintroduced by Ville for signal analysis.[32–34] WVD has been established in other branches of science which rely heavily on noise analysis as the quasi standard to conduct such analyses. In this work, the theoretical mathematical background of different time-frequency methods is reviewed first in order to make the later parts understandable. At the same time, different practical advantages and disadvantages of the different methods shall be briefly described. It is to be understood, however, that this treatment cannot replace a deeper reading of the references cited there if one wants to apply these techniques. In electrochemistry, WVD was previously employed only to a limited extend for the quantitative analysis of the stationarity of EN data and to investigate the process of electrodissolution of metals.[22]

EN records used in this paper were obtained on AA1080 and AA6016 in a range of solutions and immersion times at open circuit potential (OCP) in order to compare extracted parameters with known features from pit formation and repassivation in these systems.

2 Theoretical background of time-frequency transforms

2.1 General considerations

Joint time-frequency distribution shows how the "energy" of a signal is distributed over time and frequency.* Energy E of the signal $x(t)$ as function of time t can be calculated by integration of either the instantaneous power $|x(t)|^2$ over time,[35]

$$E = \int_{-\infty}^{+\infty} |x(t)|^2 \mathrm{d}t, \tag{1}$$

or the energy spectral density $|X(f)|^2$ over the frequency[35],

$$E = \int_{-\infty}^{+\infty} |X(f)|^2 \mathrm{d}f. \tag{2}$$

A real signal $x(t)$ exhibits Hermitian symmetry between the positive-frequency and negative-frequency components of its spectrum. The power spectral density, $S(f)$, of a signal is defined as the Fourier transform of its auto-correlation function $R(\tau)$,

$$S(f) = \int_{-\infty}^{+\infty} R(\tau)^{-\mathbb{i}2\pi f\tau} \mathrm{d}\tau, \tag{3}$$

with lag time τ and $\mathbb{i} = \sqrt{-1}$. $R(\tau)$ is the kernel for the WVD, which will be used later throughout this paper.

One can thus define a joint time-frequency energy density $\rho(t, f)$, the integration of which also yields the energy,

$$E = \iint_{-\infty}^{+\infty} \rho(t, f) \mathrm{d}t\mathrm{d}f \tag{4}$$

The joint time-frequency energy density must satisfy the marginal conditions

$$|X(f)|^2 = \int_{-\infty}^{+\infty} \rho(t, f) \mathrm{d}t \tag{5}$$

and

$$|x(t)|^2 = \int_{-\infty}^{+\infty} \rho(t, f) \mathrm{d}f, \tag{6}$$

which indicate that the integration of the joint time-frequency energy density over the frequency gives the square modulus of the signal, $|x(t)|^2$, instantaneous power, and the integration over the time gives the energy spectrum, $|X(f)|^2$.[36]

2.2 Short-time Fourier transform (STFT)

The extensively used STFT method is a linear time-frequency representation that decomposes signals by taking Fourier transforms over a sliding time window as[37]

$$STFT(t, f) = X(\tau, f) = \int_{-\infty}^{+\infty} x(t) h(t-\tau)^{-\mathbb{i}2\pi f t} \mathrm{d}t \tag{7}$$

where $h(t)$ is a short time analysis window centered around $t = 0$ and $\nu = 0$. The frequency resolution can be defined as the spacing between data points in frequency, while the adequate time-frequency resolution is achieved by choosing the proper window length about the same size as the time-invariance of the individual signal components.Time-frequency resolution of STFT is governed by the Heisenberg uncertainty principle.[32] Due to this relationship, high spectral resolution can only be achieved with relatively long windows, which inevitably results in a loss of temporal resolution. STFT has low computational complexity and can be used to determine the general time-frequency structure of the noise signal.

2.3 Wavelet transform (WT)

A wavelet is an oscillatory, finite length, real or complex function of zero mean. The WT method is also a linear time-frequency representation where a short time oscillating function $\psi(t)$ designated as "mother wavelet" is used instead of short time analysis window $h(t)$. The integral wavelet transform of the signal can be written as

$$WT_x(t, a) = \frac{1}{\sqrt{a}} \int_{-\infty}^{+\infty} x(\tau) \psi\left(\frac{t-\tau}{a}\right) \mathrm{d}\tau, \tag{8}$$

*This work follows the terminology used in signal processing, in which "power" is the squared modulus of the signal, and "energy" the integral over the signal with time as defined in eq. (1). In other words, power and energy in this context are not the physical quantities of energy and power.

where τ is time translation, a is time dilation and $1/\sqrt{a}$ is a normalization factor.[38] Compression and expansion of the mother wavelet are referred to as "scaling", where a is the scale parameter, which acts as a pseudo-frequency. It shrinks or stretches the wavelet as it is translated along time, leading to a variable resolution. The squared modulus of WT, referred to as "scalogram", reveals the energy distribution in the scale-time plane.

In electrochemistry, continuous wavelet transform (CWT) and discrete wavelet transform (DWT) are often applied as tools for denoising, baseline drift removal and separation of overlapping transients.[23,39] The most relevant feature of WT is its capability of decomposing EN records into a sum of scaled and shifted versions of the wavelet function called wavelet coefficients, which contain information, e.g., about corrosion events occurring on different timescales. The time record $x_n, (n = 1, \ldots, N)$ is decomposed using a linear combination of functions which are derived from the father wavelets $\Phi_{i,k}$ and the mother wavelets $\psi_{i,k}$ through scaling and translation as

$$x(t) = \sum_i d_{1,k}\psi_{1,k}(t) + d_{2,k}\psi_{2,k}(t) + \ldots + d_{i,k}\psi_{i,k}(t) + a_{i,k}\Phi_{i,k}(t), \quad (9)$$

where $a_{i,k}, d_{1,1}, \ldots, d_{i,k}$ are the wavelet coefficients, $k = 1, 2, \ldots, N/2^i$, and $i = 1, 2, \ldots, I$, where I is a small natural number which depends on the number of analysed data N and the functions which are derived from the father wavelets and the mother wavelets.

The mother and father wavelets are given as

$$\psi_{i,k}(t) = 2^{-\frac{i}{2}}\psi\left(\frac{t - 2^i k}{2^i}\right), \quad (10)$$

and

$$\Phi_{i,k}(t) = 2^{-\frac{i}{2}}\Phi\left(\frac{t - 2^i k}{2^i}\right). \quad (11)$$

The signal can also be decomposed into partial signals, known as "crystals",

$$x(t) = D_1(t) + D_2(t) + \ldots + D_i(t) + A_i(t) \quad (12)$$

where $D_1(t), \ldots D_i(t)$ are crystals that can be obtained by inverse DWT. Crystals are partial signals that describe $x(t)$ on a particular timescale covering a specific frequency range. The approximation signal $A_i(t)$ contains the general trend of the signal and by subtracting it from $x(t)$ one eliminates the DC drift from the time record. The "fast wavelet transform" algorithm is used for the computation of DWT in practice. Signals are analyzed at different scales by using different low-pass and high-pass filters. The high frequency component of the signal (the detail) is collected through a series of high-pass filters, while the application of series of low-pass filters is used to retain the low frequency component. After filtering and down-sampling the signal is decomposed into the detail coefficients, $d_1, d_2 \ldots, d_I$ and the smooth coefficients a_I, containing the information about the local fluctuations and the general trend of the signal, respectively. The scale range that covers certain crystals can be approximated as

$$(D_1^{(\mathrm{i})}, D_2^{(\mathrm{i})}) \approx 2^i \Delta t, 2^{i-1}\Delta t \quad (13)$$

where Δt is the sampling interval and i is the crystal level. The scale range can be used to approximate pseudo-frequencies, $\nu = \nu_0/a$, where a is a scale, and ν_0 is the central frequency (ν_0=0.7143 Hz for db4 wavelets).[24] The energy content of each scale normalized to the total energy in the signal can display the dominant corrosion events occurring in the investigated system.[30,40,41] The energy of the whole signal is[42]

$$E = \sum_{n=1}^{N} x_n^2. \quad (14)$$

The energy contained within detail and approximation coefficients, respectively, is[42]

$$E_i^{(\mathrm{d})} = \frac{1}{E}\sum_{n=1}^{\frac{N}{2^i}} d_{i,n}^2 \qquad i = 1 \ldots I \quad (15)$$

where i stands for the corresponding crystal, and

$$E_I^{(\mathrm{a})} = \frac{1}{E}\sum_{n=1}^{\frac{N}{2^i}} a_{I,n}^2. \quad (16)$$

Because the chosen wavelets are orthogonal, the equation

$$E = E_I^{(\mathrm{a})} + \sum_{i=1}^{I} E_i^{(\mathrm{d})} \quad (17)$$

is satisfied.

2.4 Wigner-Ville distribution

Time-frequency representations can be expressed in terms of the general family of bilinear time-frequency distribution representations known as Cohen's class representations,[43]

$$\rho(t, f) = \quad (18)$$

$$\iint_{-\infty}^{+\infty} e^{\mathrm{i}2\pi\nu(u-t)}\Omega(\nu, \tau)\, x_{\mathrm{a}}\left(u + \frac{\tau}{2}\right) {x_{\mathrm{a}}}^*\left(u - \frac{\tau}{2}\right)^{-\mathrm{i}2\pi f\tau} \mathrm{d}\nu \mathrm{d}u \mathrm{d}\tau,$$

where $\Omega(\nu, \tau)$ is the parameterization function that determines the characteristics of the time-frequency distribution, and * indicates the complex conjugate. The properties of a particular distribution are reflected by constraints on the kernel. Cohen's class includes a large number of the existing time-frequency energy distributions. The WVD (and all of Cohen's class of distributions) uses a variation of the autocorrelation function where time remains in the result, called instantaneous autocorrelation function. The WVD is obtained by setting $\Phi(\nu, \tau) = 1$. In this representation, $x(t)$ is used in the form of its analytic associate $x_{\mathrm{a}}(t)$, which is defined by its Hilbert transform $H[x(t)]$ and presents a signal without negative frequency components,[44,45]

$$x_{\mathrm{a}}(t) = x(t) + \mathrm{i}H[x(t)]. \quad (19)$$

Because of the Hermitian symmetry, no information is lost in the transformation process. The Hilbert transform is used for obtaining the instantaneous envelope and frequency (IF) of a time series. The IF is a basic parameter which may be used to describe

the nonstationarity in a process and can be defined as the time rate of change in the instantaneous phase angle.[46] WVD is actually the Fourier transform of the signal's autocorrelation function with respect to the time delay variable,

$$WVD_x(t,f) = \int_{-\infty}^{+\infty} x_a\left(t+\frac{\tau}{2}\right) {x_a}^*\left(t-\frac{\tau}{2}\right)^{-i2\pi f\tau} d\tau. \quad (20)$$

WVD gives the energy density of various frequency components at given times. A WVD is always real-valued, time and frequency covariant and satisfies the marginal properties given in eq. (5) and (6). The main drawback of this time-frequency transform is generation of cross-terms. Cross-terms are artifacts that appear in the WVD and falsely indicate the existence of signal components between actual signals. Their presence can hinder the readability of the obtained spectra, but they also contain some additional information about the investigated signal. The major motivation for smoothing the WVD is that many of the cross-terms are suppressed.[37]

The pseudo-WVD (PWVD) can be represented as a WVD smoothed with a short time window $h(\tau)$,

$$PWVD_{h,x}(t,f) = \int_{-\infty}^{+\infty} x_a\left(t+\frac{\tau}{2}\right) {x_a}^*\left(t-\frac{\tau}{2}\right) h(\tau)^{-i2\pi f\tau} d\tau \quad (21)$$

The window width should be smaller than the typical scale of the fluctuation of interest. Likewise, the smoothed pseudo WVD (SPWVD) almost completely suppresses cross-terms artifacts but with lower resolution compared to the original WVD. Here, an additional window function is added so that smoothing in time and frequency can be adjusted independently,

$$SPWVD_{g,h,x}(t,f) = \iint_{-\infty}^{+\infty} x_a\left(t+\frac{\tau}{2}\right) {x_a}^*\left(t-\frac{\tau}{2}\right) g(\nu) h(\tau)^{-i2\pi f\tau} d\nu d\tau, \quad (22)$$

where ν is the frequency offset, $g(\nu)$ is the time smoothing window and $h(\tau)$ the frequency smoothing window. Compared to the WVD the cross-terms will be attenuated, but some properties of the WVD will be lost, such as the marginal properties, the unitarity, and also the frequency-support conservation.[47]

In order to further improve the spectra in terms of readability, a reassignment-based methodology was proposed.[37] To further describe this method, it is convenient to express Cohen's class as

$$\rho_x(t,f) = \iint_{-\infty}^{+\infty} \Pi(u-t,\nu-f) WVD_x(u,\nu) du d\nu, \quad (23)$$

where the arbitrary kernel $\Pi(\nu,\tau)$ is the two-dimensional Fourier transform of parametrization function $\Phi(\nu,\tau)$. This method assigns the energy content to a new point within the time-frequency plane. The reassignment procedure creates a modified version of the TFR based upon moving the computed center of gravity of the signal power around t and f to new coordinates $\hat{t}$ and $\hat{f}$ such that

$$\hat{t}(x;t,f) = \frac{\iint_{-\infty}^{+\infty} u\Pi(u-t,\nu-f) WVD_x(u,\nu) du d\nu}{\iint_{-\infty}^{+\infty} \Pi(u-t,\nu-f) WVD_x(u,\nu) du d\nu} \quad (24)$$

and

$$\hat{f}(x;t,f) = \frac{\iint_{-\infty}^{+\infty} \nu\Pi(u-t,\nu-f) WVD_x(u,\nu) du d\nu}{\iint_{-\infty}^{+\infty} \Pi(u-t,\nu-f) WVD_x(u,\nu) du d\nu}. \quad (25)$$

This distribution reduces the cross-terms of the WVD. The reassigned WVD at any point (t',f') is therefore the sum of all the spectral values moved to this point,

$$RSPWVD_x(t',f') = \iint_{-\infty}^{+\infty} \rho_x(t,f)\sigma\left(t'-\hat{t}(x;t,f)\right)\delta\left(f'-\hat{f}(x;t,f)\right) dt df \quad (26)$$

where $\delta(t)$ represents the Dirac δ distribution. The aim of the reassignment method is to achieve both reduction of the cross-terms and an improved sharpness of the signal components by reallocating its energy distribution in the time-frequency plane.[37] The modified representation preserves the time and frequency shift invariance, the energy conservation and provides the sharp localization but no longer belongs to Cohen's class due to lost bilinearity.

3 Materials and methods

The time records of current and potential were recorded in a three electrode configuration with two nominally identical working electrodes. Experiments were conducted on AA1080 (99.8%, "industrially pure" Al) and AA6016 at OCP. The electrodes of working area of 1.2 cm^2 were wet ground up to 1000-grit carbide paper. A saturated Ag/AgCl was used as the reference electrode in both setups. AA1080 electrodes were first passivated in a borate buffer (pH=6.4), for 24 h. After passivation, NaCl was added so that the final concentration became 0.1 M NaCl in the solution. Prior to experiments AA6016 was annealed by heating to 560°C. This process enhances the final mechanical properties of the alloy and generates a thick oxide layer on the surface, because of the rearrangement of the surface crystalline structure. After annealing AA6016 was exposed to 0.1 M NaCl solution for 24 h. Electrochemical current (ECN) and potential (EPN) noise were collected at OCP. The electrolyte solution was not stirred and kept at a temperature of 25°C, controlled by a thermostat. Current and potential signals were recorded using Ivium-n-Stat potentiostat working as zero resistance ammeter (ZRA) and potentiometer. This type of potentiostat was successfully used before for EN analysis by other research groups.[25,26,30,48–50] The sampling frequency used for all the measurements was varied from 1 Hz to 10 Hz with a 10 Hz low-pass filter. In order to validate the EN measurement system, EN measurements with dummy cells have been performed at 3 sampling frequencies to control the overlap of the PSDs in common frequency ranges. This validation procedure has been detailed in a guideline for assessing EN measurement devices.[51]

Prior to time-frequency analysis, several data treatment steps have been performed. The first step in data analysis was to remove the DC component from the EN signals. For this purpose, DWT was employed using the orthogonal Daubechies wavelet, db4, with 10 levels of decomposition. In this work, the DWT was

chosen for the baseline removal since it offers good representation of nonstationary signals and efficient trend removal without removing the useful information present in the data.[30] The application of wavelet trend removal was demonstrated to be superior when compared to moving average, polynomial or linear trend removal.[30] After trend subtraction, to remove cross-terms from the time-frequency distribution, the analytic associate of the signal was calculated by performing the Hilbert transformation. The data were processed using Matlab from MathWorks. The CWT was computed with an analytic Morlet wavelet. The WVD were obtained by the Time-Frequency Toolbox (TFTB) for the analysis of non-stationary signals using time-frequency distributions developed by F. Auger et al.[47]. The raw data, and the analysis scripts for RSPWVD method are available in a data package associated with this work.[52]

The energy distribution plots (EDP) and energy spectral densities (ESD) were also calculated for all the investigated systems to compare with the obtained results from RSPWVD and DWT.

4 Results and discussion

4.1 Comparison of time-frequency transforms

The purpose of this section was to compare different time-frequency transforms applied to spectral decompositions of EN data. As shown in Figure 1, we conducted STFT, CWT, PWVD, SPWVD and RSPWVD spectral decomposition of the EPN record obtained on AA6016 after 24 h immersion in 0.1 M NaCl to induce pitting on the sample surface surface. Under these conditions at ambient temperature, pitting attack is expected to occur.[53,54] The Cl^- ions can prevent oxide film formation by adsorbing or incorporate into an already formed oxide, by changing the activity of hydrogen ions in pits, and by forming a layer of salt at the pit bottom.[55] All the spectra were normalized to [0,1] to facilitate comparison. Figure 1 shows data in the frequency range up to 1 Hz, where most of the features were observed. WVD can yield negative values, which would correspond to a negative energy. As this is not physically possible following the definitions in eq. (1), (2) and (4), only the positive values were considered in the spectra based on WVD.[56]

Figure 1a shows the potential fluctuations recorded at OCP with few transients that are easy to distinguish visually. Transients have a sharp potential change, corresponding to pit initiation and growth. The termination of the pit growth is followed by slower potential recovery, corresponding to repassivation or film growth and discharge of the interface capacity of the repassivated surface.[57]

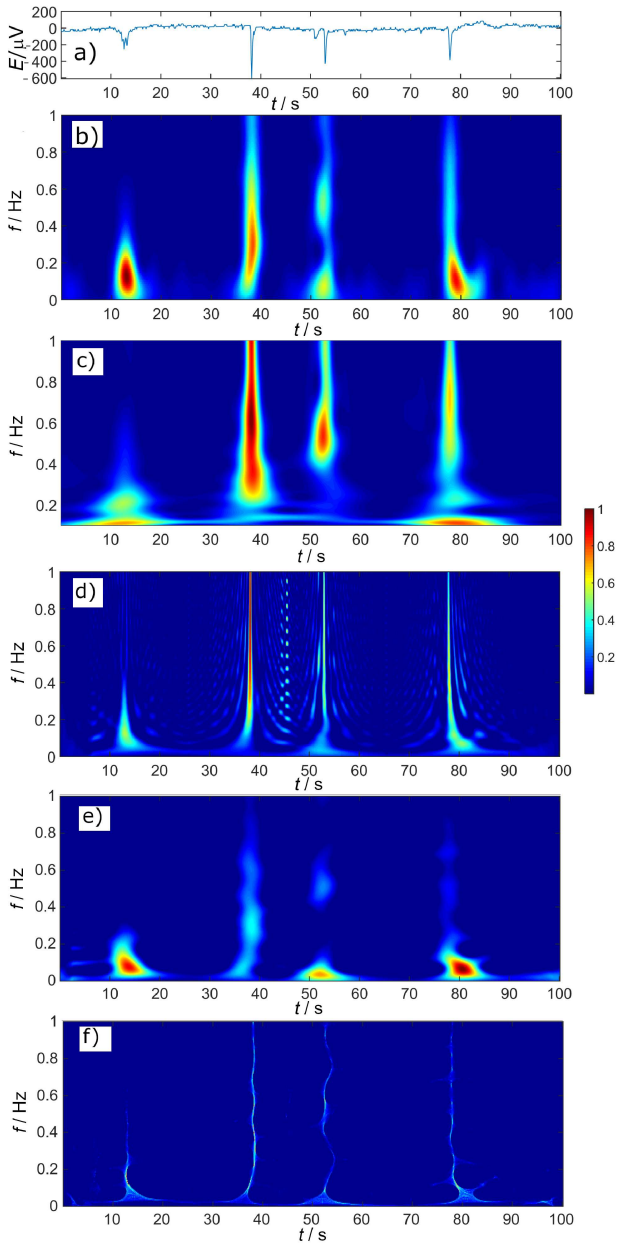

Fig. 1 Time-frequency spectra of a) EPN time record, obtained with different methods of spectral decomposition b) STFT, c) CWT, d) PWVD, e) SPWVD, f) RSPWVD on AA6016 in 0.1 M NaCl, after 24 h immersion

For STFT results presented in Figure 1b, a Hamming window of length 15 s was applied. Such a short window allows good resolution with respect to time, while the frequency resolution is reduced. Due to time-frequency windows of short time, STFT offers limited resolution in both time and frequency domain. At this window length, the resolution of STFT was approximately 70 mHz, while the temporal resolution was close to 8 s when looking at the group of transients occurring at about 13 s. However, the main drawback of STFT is the right choice of the window length to achieve sharp localization in time and frequency simultaneously, i.e. the necessary trade-off between time and frequency resolutions. The STFT is relatively simple, but mostly suitable for

stationary signals. STFT provided certain discrimination between signal frequency components when looking at the transients occurring at about 53 s This comparison showed that even with a compromise window length, resolution in both time and frequency domains was lower compared to the methods based on WVD.

CWT, on the other hand, employs a size-adjustable window, which is beneficial compared to the fixed window used by STFT. CWT consequently provided better spectral resolution compared to STFT and yielded more details (Figure 1c). The frequency resolution here was approximately 10 mHz. However, time localization for the dataset in this study was rather poor, as the transients occurring at 13 s and 79 s were smeared out significantly.

Application of PWVD (Figure 1d) yielded enhanced spectral and temporal resolution compared to both STFT and CWT. However, the spectra suffered from the presence of spurious energy terms. PWVD (Figure 1d) provided good spectral resolution close to 5 mHz while the SPWVD (Figure 1e) significantly reduced the spurious energy terms from PWVD. STFT and SPWVD could distinguish between the two components of the signal when looking at the group of transients occurring at about 53 s, however, STFT showed a higher leakage between the two frequency peaks compared to the SPWVD. The thick energy band obtained by SPWVD was making small frequency variations difficult to distinguish, while RSPWVD (Figure 1f) provided an enhanced concentration of the signal components and followed in more detail the frequency variations, with a resolution higher than 1 mHz and temporal resolution around 0.1 s. In this paper, we have used the Hamming window set to $N/8$ and $N/4$ for time and frequency smoothing windows, respectively, where N is the number of recorded samples. Shorter smoothing windows will give more details, especially when it comes to high-frequency signals, but also introduce more artifacts. RSPWVD removed the majority of interferences and enabled good frequency and temporal resolution. From all methods used here, RSPWVD provided the lowest spectral width of the features, and at the same time the lowest temporal width. In the time domain, regions with wide spectral features coincided with observed sharp transients in EPN. Thus, RSPWVD was chosen to analyze the data in more detail.

4.2 Application of RSPWVD to study the breakdown of Al passivity

In this section, the applicability of RSPWVD for the analysis of EN measurements will be discussed in more detail on EN records obtained on Al electrodes under different conditions. EN measurements are used to study Al covered by passive films and the changes in the signal that occur when the passive film breaks down and pitting occurs.

Electrodes made of AA1080 were passivated in a borate buffer (pH=6.4) for 24 h at OCP. After passivation, NaCl was added to the solution to induce a localized attack. ECN was recorded at OCP after 5 h of exposure of 1080 electrodes in solution. In a second set of experiments, electrodes made of AA6016, annealed by heating to 560°C, were exposed to unbuffered 0.1 M NaCl solution for 24 h at OCP. Figure 2 and Figure 3 show ECN (a) and

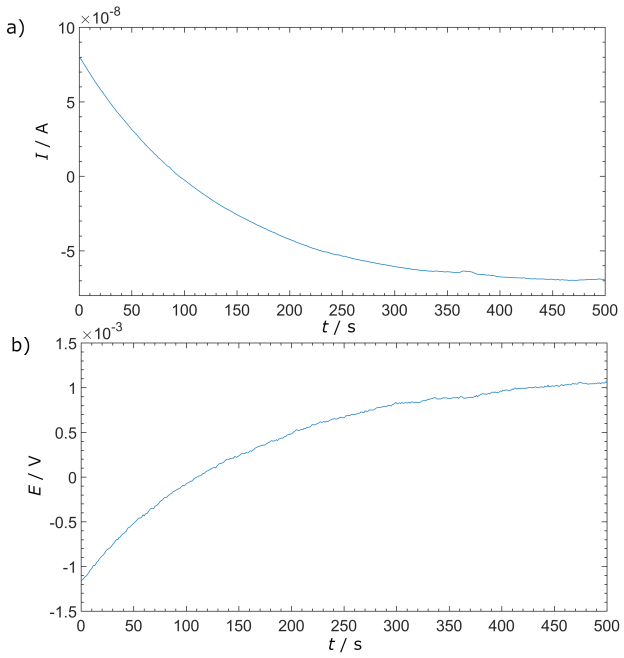

Fig. 2 Time records of a) ECN and b) EPN of AA1080 in borate buffer after 24 h of exposure under OCP.

EPN (b) recorded at OCP and their corresponding RSPWVD in a two-dimensional contour plot, respectively. The ECN record (Figure 2a) is flat without any prominent transients and within 0.3 μA current range, while the EPN fluctuations (Figure 2b) reach up to 5 mV drift from zero. In neutral noncomplexing solutions, the oxide film on aluminum has very low solubility, and low conductivity, blocking most of the redox reactions. Al oxide films grown in a borate solution are reported to be thin, dense, coherent and amorphous.[55] An amorphous passive film is generally considered more protective than a crystalline one due to lower tendency to localized breakdown because of its uniform structure.[58] The passive film has a dynamic structure and the breakdown of the passive film is the initial stage of the pitting process. In RSPWVD time-frequency spectra of ECN and EPN (Figure 3a and b), one notices the absence of high frequency events as well as the presence of a low intensity and a low frequency events (below $5{\cdot}10^{-3}$ Hz). This absence indicates the occurrence of long timescale processes and the presence of a passive oxide film. The presence of these processes on larger timescales in the EPN spectra can be explained by the slow potential drift or as the discharge of the passivated surface. The low magnitude of RSPWVD result and the absence of current and voltage transients indicate the expected Al passivity. Figure 4 and Figure 5, respectively, show ECN (a) and EPN (b) records and their corresponding RSPWVD spectra obtained on AA1080 in borate buffer 5 h after addition of 0.1 M NaCl. The amplitude of the current record obtained in the presence of 0.1 M NaCl (Figure 4a) exhibits approximately 1.5 μA current range with significant increase in the noise levels, with occurrence of many transients. Accordingly, the EPN fluctuations reached up to 10 mV potential range. In the RSPWVD spectrum of ECN (Figure 5a) many overlapping transients can be

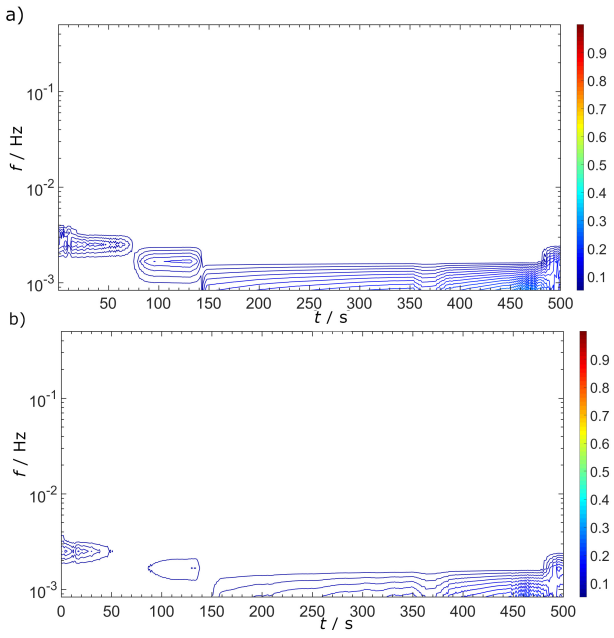

Fig. 3 Time-frequency spectra of a) ECN and b) EPN of AA1080 in borate buffer after 24 h of exposure under OCP obtained with RSPWVD.

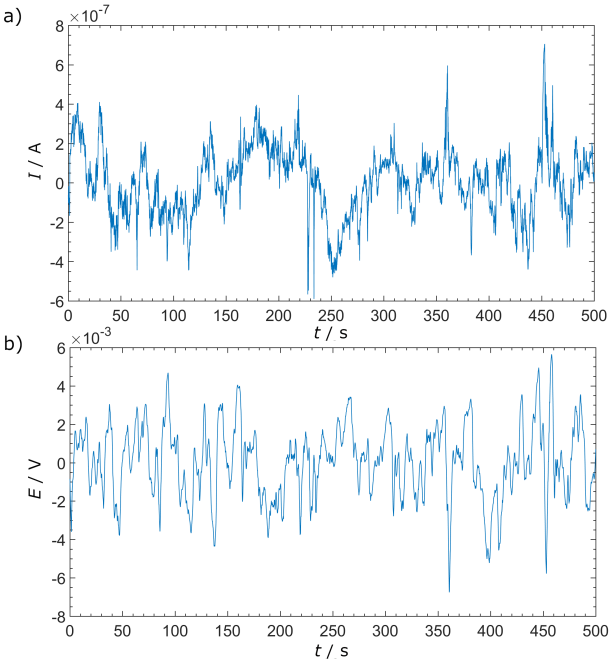

Fig. 4 Time records of a) ECN and b) EPN of AA1080 in borate buffer with 0.1 M NaCl after 5 h at OCP.

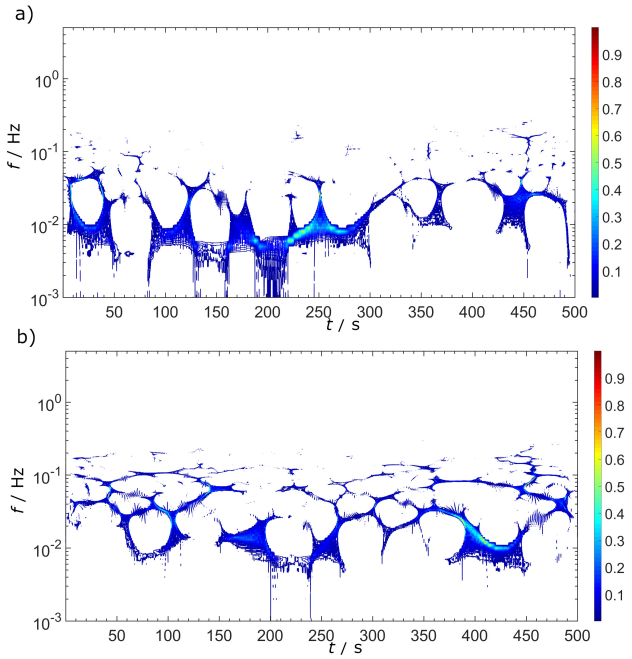

Fig. 5 Time-frequency spectra obtained with RSPWVD of a) ECN and b) EPN of AA1080 in borate buffer with 0.1 M NaCl after 5 h at OCP.

observed. The transients in the ECN record occurring at ≈30 s, 250 s and 450 s in the frequency range from 10^{-2} to 10^{-1} Hz are exhibiting high energy content and probably indicate the breakdown of the passive layer in the presence of Cl^- ions. In line with this interpretation, the larger time constant events in Figure 5 can be attributed to the increase in the lifetime of the metastable pits and transition towards more stable pitting. Pitting of Al involves repeated breakdown-repair events.[58,59]

Pure aluminium from 1xxx series is more resistant to some types of corrosion than other alloys, although its corrosion resistance can vary with the change in alloying content. In pH range 4 to 9 where the oxide is stable, Al is reported to be subject to only localized pitting corrosion.[60] Pitting is considered to be a self-accelerating process where the local pit environment becomes depleted of cathodic reactant. Consequently the pit environment becomes enriched in metal cations and anionic species (e.g. Cl^-) are being transported into the pit to provide charge neutrality and thereby creating acidic environment that ensures a propagation of pit growth. Chloride is a small anion with a high diffusivity, that is well known to interfere with passivation.[61] Metastable pitting is in general characterized by current fluctuations occurring prior to the pitting corrosion of metals corresponding to small pits in an early stage of development.[61] It is further well known that metastable pits initiate at potentials far below the critical pitting potential.[61]

Figure 6 and Figure 7 show ECN and EPN time records and corresponding RSPWVD spectra, respectively, obtained on AA6016 immersed in 0.1 M NaCl for 24 h.

The raw ECN record obtained before detrending was positive within a 2 μA dynamic range. On the other hand raw EPN record obtained before detrending was negative within approximately

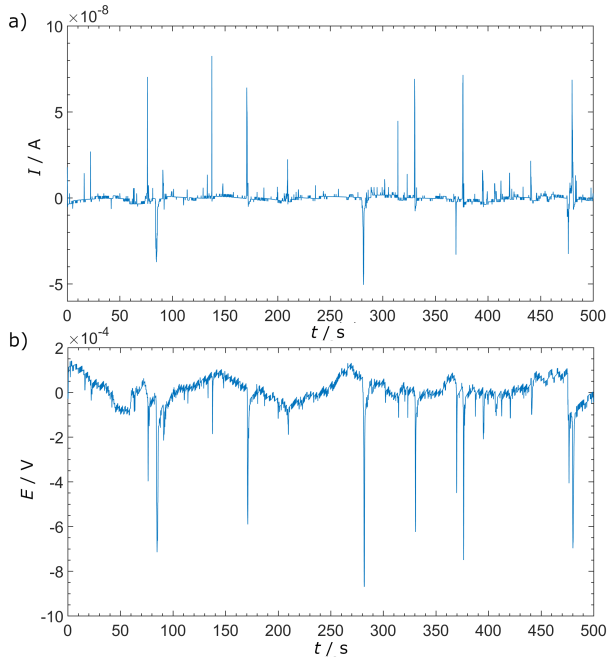

Fig. 6 Time records of a) ECN and b) EPN of AA6016 in 0.1 M NaCl after 24 h at OCP.

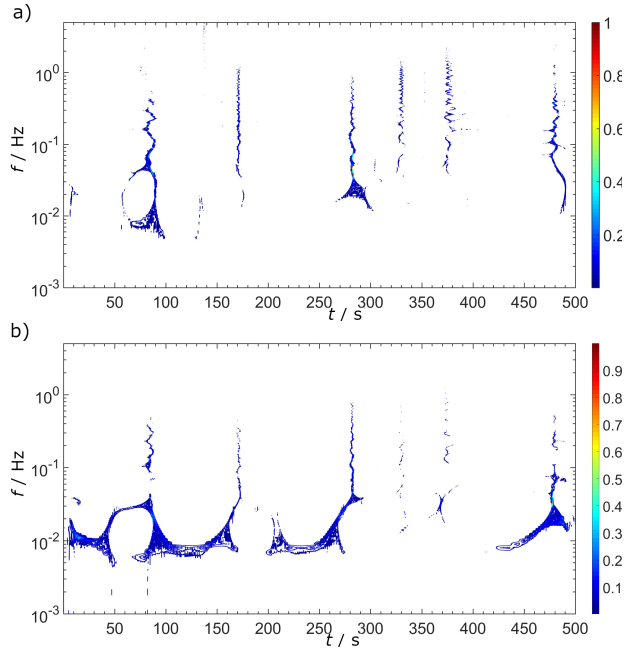

Fig. 7 Time-frequency spectra obtained with RSPWVD of a) ECN and b) EPN of AA6016 in 0.1 M NaCl after 24 h at OCP.

5 mV dynamic range. The ECN signal shows positive and negative transients consistent with pitting on both measuring and counter electrode. In addition, the EPN signal shows also a pattern characteristic for ongoing pitting corrosion. Different shapes of current transients may be observed. Isolated transients of both EPN and ECN have decay times in the range between 1 and 3 s.

Depending on metal and corrosive environment, the net anodic current associated with a metastable pits can have different forms.[62] The decay times of the current bursts is reported to correspond to the maximum repassivation times.[63] Passive films were reported to always be in a state of breakdown and repair as the result of nucleation, short growth and repassivation of a micropit on the surface.[63] Nucleation and growth of metastable pits are important processes for understanding the transition from metastable to stable pitting. Observed transients in ECN (Figure 6a) decreased approximately exponentially with time, which can be associated with discrete pitting events.[64] Only pits that survive metastable pitting become stable growing pits.[61]

Aluminum alloys have a heterogeneous structure composed of an Al-rich matrix and secondary phase particles. The variations in electrochemical properties of these elements may introduce local electrochemical cells in the material which can make the Al alloys susceptible to corrosive attacks.[65]

Cathodic events in ECN (Figure 6a) observed at 85 s, 280 s and 475 s show multiple peaks, which is reported to correspond to the dissolution of active secondary phase particles that can disrupt the oxide film.[66] The spectra presented in Figure 7 enable us to determine the frequency contribution of individual transients.

The cathodic transient at approximately 85 s and 0.05 Hz is showing the energy amplitude approximately 5 times lower as compared to the cathodic transient occurring at 280 s at 0.05 Hz. On the other hand, anodic transients at 480 s with maximum at a frequency of 0.1 Hz shows 2.5 times higher energy content as compared to anodic transients at 380 s and exhibits the frequency of approximately 0.3 Hz at the amplitude maximum as read from RSPWVD. The frequency distribution in the spectrum obtained by RSPWVD (Figure 7) indicated the initiation of localized processes on the electrode surface, which were characterized by instantaneous frequencies between 10^{-2} to 1 Hz.[67]

The observed difference confirms that RSPWVD can provide quantification of each individual event recorded. RSPWVD proves to be sensitive to the differences existing between two similar processes of similar magnitude. The delay at the lower potential in EPN transients at about 370 s and 475 s is reported to be indicative of a pit growth at a slower rate as compared to propagation/repassivation phase.[68] The formation of a pit causes an ohmic potential drop in solution.[62]

Difference in the noise pattern obtained on AA1080 in borate buffer 5 h after addition of 0.1 M NaCl (Figure 5), and obtained on AA6016 immersed in 0.1 M NaCl for 24 h (Figure 7) can be explained by the influence of different alloying elements on the protectiveness of the passive film. The alloy composition and microstructure can also have strong effects on the tendency for an alloy to pitting. Two main alloying elements of AA6016 are Mg and Si. The variations in electrochemical properties of these elements may introduce local electrochemical cells in the material which

make the alloys susceptible to localized corrosion attacks.[69] In addition AA6016 was also thermally treated with solution heat treatment and aging to attain the desired mechanical properties. The heat treatment of the alloy will affect the corrosion resistance of the material. Pitting can also initiate by local alkalisation near cathodic inclusions, caused by intermetallic particles.[70] Stable pits survive the metastable stage and continue to grow, whereas metastable pits repassivate and stop growing. It is believed that that metastable pit growth is under ohmic control as a result of the resistance associated with the porous pit cover. Therefore, the increase in the energy of low frequency components for AA1080 (Figure 5) could also indicate the onset of slower processes on the surface, such as diffusion-controlled growth of pits and salt nuclei on the surface.[71,72] Furthermore, the current amplitudes shifted to higher values probably due to the stabilization of individual pits.[72] On the other hand, noise spectrum of AA6016 (Figure 7) shows higher values of instantaneous frequencies.

Metastable pits are typically considered to be those of micron size at most with a lifetime on the order of seconds or less.[73] Repassivation includes both pit solution dilution and film growth and occurs within times ranging from several to tens of seconds.[67] It has been reported that when stable pits are small, they behave identically to metastable pits.[61]

EPN and ECN data which was collected was transformed into ESD plots for the whole measurement time. The ESD plots were calculated from the RSPWVD after trend removal with DWT. ESDs are used to characterize the corrosion process in the frequency domain. To facilitate interpretation of the frequency characteristics, two dimensional representations are used here. ESD contains information about the sum of the amplitudes of the noise signal at each time, and allows the quantification of the intensity and the mechanism of the corrosion process. In Figure 8 and 9 the ESD of ECN and EPN of different samples at OCP are presented.

ESD plots of ECN (Figure 8a) and EPN (Figure 9a) signals of AA1080 in borate buffer after 24 h exposure are clearly demonstrating the contribution of very low frequency components around 10^{-3} Hz. On the other hand, ESD plot of ECN and EPN record (Figure 8b and Figure9b) obtained on AA1080 in the borate buffer in the presence of 0.1 M NaCl after 5 h exposure demonstrate the contribution of the frequency components between 10^{-2} and 10^{-1} Hz and increased severity of the corrosion process compared to AA1080 in borate buffer. Furthermore, ESD plot of ECN and EPN record (Figure 9b Figure 9c) obtained on AA6016 in the presence of 0.1 M NaCl after 24 h of immersion further clearly demonstrate the significant increase in the contribution of the frequency components between 10^{-1} and 1 Hz.[74]

In continuation, EDP plots obtained from DWT are often used to discriminate between different corrosion types.[39] Each crystal in EDP gives some information about prevalent physicochemical processes. The position of the peak in the EDP plot indicated the dominant frequencies in certain corrosion events and its change may indicate the dominant corrosion process.[24] In Figure 10 and Figure 11 the EDP plots of ECN and EPN signals on all samples under OCP are shown separately.

EDP plots are used as an additional method to verify the results obtained by RSPWVD. In addition EDP and ESD plots from

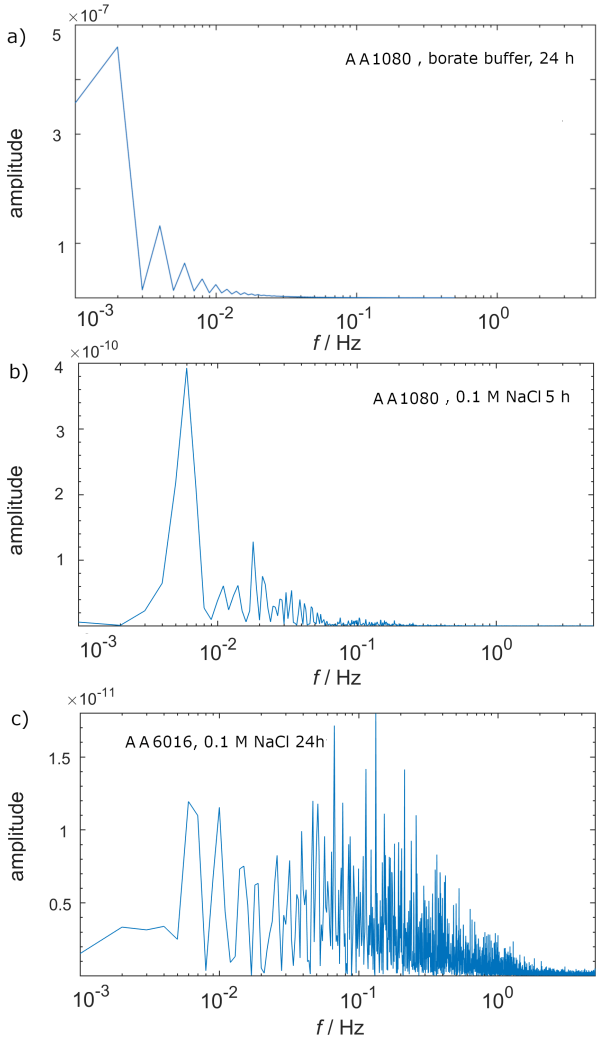

Fig. 8 ESD plots obtained from RSPWVD of ECN of a) AA1080 in borate buffer after 24 h and b) AA1080 in borate buffer with 0.1 M NaCl after 5 h and c) AA6016 in 0.1 M NaCl after 24 h at OCP.

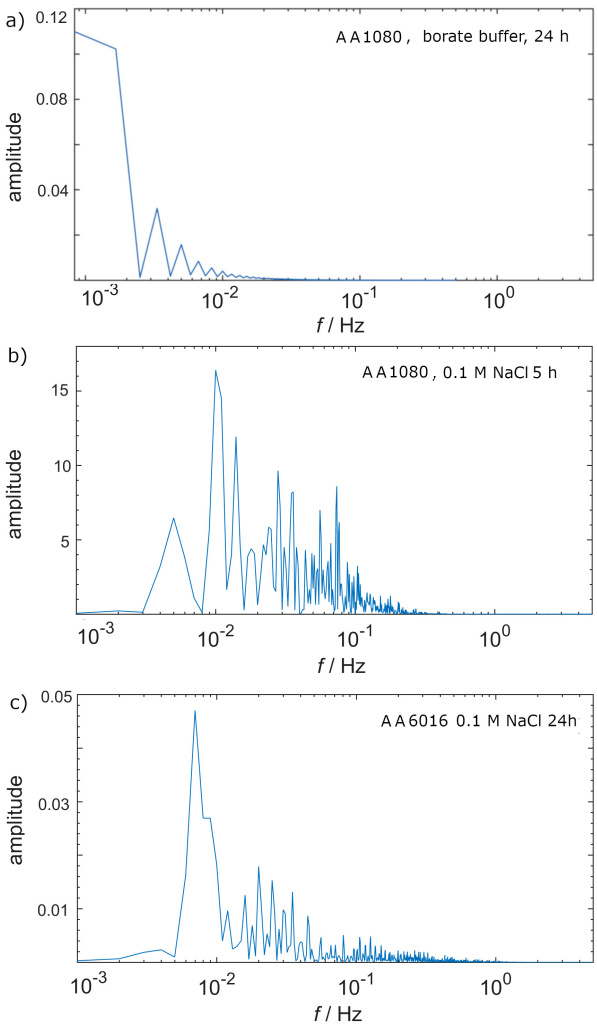

Fig. 9 ESD plots obtained from RSPWVD of EPN of a) AA1080 in borate buffer after 24 h and b) AA1080 in borate buffer with 0.1 M NaCl after 5 h and c) AA6016 in 0.1 M NaCl after 24 h at OCP.

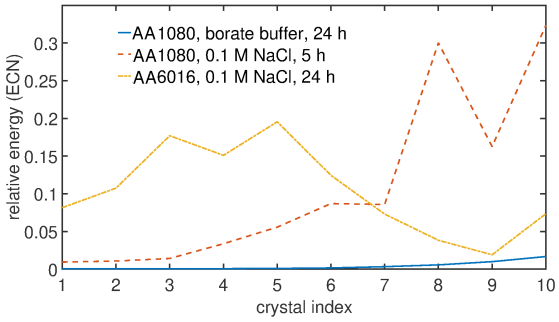

Fig. 10 EDP plots obtained with DWT of ECN of all the samples in different electrolytes.

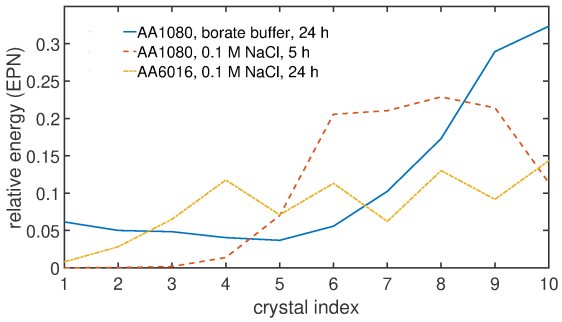

Fig. 11 EDP plots obtained with DWT of EPN of all the samples in different electrolytes.

RSPWVD can be easily compared.

In the ECN signals of AA1080 in borate buffer the energy was stored predominantly in the higher crystals D9-D10, which correspond to a large timescale. In the obtained time records (Figure 2a and Figure 2b), these were characterized mainly by a very slow drift. The ECN recorded in the presence of 0.1 M NaCl displayed an increase in the relative energy of the crystals, and particularly crystal D8, corresponding to larger timescales, and a peak at D6 corresponding to medium timescales.

The high values for the relative energy of crystals D8, D9 and D10 reveal the fact that transients with a large time constant prevailed over those with a medium one in the ECN signal. Dominance of large and medium time constant processes is in accordance with the dominant frequency contribution from 10^{-2} to 10^{-1} Hz in the RSPWVD spectra. Long timescale crystals indicate diffusion-controlled processes, which can be present in general corrosion. In EDP plots of ECN records obtained on AA6016, relative energy is mostly stored in D3-D5 crystals, confirming the change in mechanism compared to AA1080 and the presence of certain localized corrosion events on the surface. Medium timescales are reported to be dominant in the case of metastable pitting.[75] The peaks in D3-D5 crystals appeared as the result of the contribution of frequencies in the range from 10^{-1} to 1 Hz. Similar observations of the main corrosion events contributing to the experimental signal were acquired by both RSPWD and DWT.

In the EPN signals of 1080 in borate buffer (figure 11) the energy was stored predominantly in the higher crystals, due to the baseline drift in the EPN signal. On the other hand EPN signals recorded in the presence of 0.1 M NaCl displayed an increase in the relative energy of the crystals D6-D9, corresponding to medium and larger timescales. EDP plots of EPN records obtained on AA6016 in the presence of 0.1 M NaCl show peaks in crystals D4, D6, D8 and D10. The increase in the lower frequency components in the EPN signals as compared to ECN signals can be due to a slower recovery of the potential after the occurrence of each transient. The difference between AA1080 and AA6016 and the decrease in the number of transients in the case of AA6016 can be further explained that crystals on medium timescales indicate the the propagation/repassivation, while the large timescale indicate the growth of pits, determined by the Ohmic resistance of the perforated pit cover and its ability to withstand diffusion.[76]

5 Conclusion

Several time-frequency transforms, as commonly used in signal processing, have been applied to the investigation of EN data of AA1080 and solution heat treated AA6016 at OCP in buffered and unbuffered Cl^--containing solutions. The RSPWVD method has been shown to be superior over other transforms more commonly applied in electrochemistry. RSPWVD permitted the estimation of the intensity of the corrosion process and the identification of the corrosion mechanism, which was demonstrated on corrosion of Al under different conditions. RSPWVD enabled a better detection of frequency changes as compared to other time-freqeuncy transforms and proved to be sensitive even to the slight differences existing between the different systems. The consistency found between the results of RSPWVD and DWT further confirmed the applicability RSPWVD for EN data analysis.

RSPWVD was used to successfully discriminate between different corrosion types. Passivity of AA1080 in borate buffer was confirmed by the absence of transients and by the presence of only slowly drifting baseline. In the presence of 0.1 M NaCl a decrease in oxide film stability was demonstrated by many overlapping transients in the frequency range from 10^{-2} to 10^{-1} Hz. RSPWVD was able to successfully detect differences existing between two different alloys. In addition RSPWVD for observed transients of AA6016 shows multiple peaks, corresponding to the dissolution of secondary phase particles. AA1080 is characterized by longer timescale processes, which probably indicate diffusion-controlled processes, or increase in the lifetime of the metastable pits and transition towards more stable pitting. On the other hand AA6016 shows decreased number of transients with contribution of frequencies in the range from 10^{-1} to 1 Hz probably due to initiation of metastable pitting. The observed difference in corrosion mechanisms between two alloys can be ascribed to the influence of alloying elements on localized corrosion and protectiveness of passive film on the metal surface. In the system investigated here, simpler analysis techniques would mostly have been sufficient to reach similar conclusions, making it a very well suited test system to compare the different time-frequency transforms. Being superior both in spectral as well as time resolution to the analysis of noise, RSPWVD may be suitable to reveal unprecedented quantitative and qualitative details of the electrochemistry of a corrosion process on a system while the process is ongoing. Importantly, 2D output such as obtained from this analysis is also highly suitable as input for machine learning algorithms that may facilitate detection of certain types of events.

Conflicts of interest

There are no conflicts to declare.

Acknowledgement

The authors are grateful to Svein Sunde for many useful discussions and to Hans-Martin Heyn for pointing out to us this particular class of time-frequency transforms. The Department of Materials Science and Engineering, NTNU, is acknowledged for financial support.

Notes and references

1 K. Hladky and J. Dawson, *Corros. Sci.*, 1981, **21**, 317–322.
2 K. Hladky and J. Dawson, *Corros. Sci.*, 1982, **22**, 231–237.
3 E. A. Astafev, A. E. Ukshe and Y. A. Dobrovolsky, *J. Electrochem. Soc.*, 2018, **165**, F604–F612.
4 R. Maizia, A. Dib, A. Thomas and S. Martemianov, *J. Solid State Electrochem.*, 2017, 1649.
5 M. A. Rubio, K. Bethune, A. Urquia and J. St-Pierre, *Int. J. Hydrog. Energy*, 2016, **41**, 14991–15001.
6 S. Martinet, R. Durand, P. Ozil, P. Leblanc and P. Blanchard, *J. Power Sources*, 1999, **83**, 93–99.
7 S. Martemianov, N. Adiutantov, Y. K. Evdokimov, L. Madier, F. Maillard and A. Thomas, *J. Solid State Electrochem.*, 2015, **19**, 2803–2810.
8 R. A. Rincón, A. Battistel, E. Ventosa, X. Chen, M. Nebel and W. Schuhmann, *ChemSusChem*, 2014, **8**, 560–566.
9 A. Zeradjanin, E. Ventosa, S. Bondarenko and W. Schuhmann, *ChemSusChem*, 2012, **5**, 1905–1911.
10 F. Huet, M. Musiani and R. Nogueira, *Electrochim. Acta*, 2003, **48**, 3981–3989.
11 Z. Zhang, W. H. Leng, Q. Y. Cai, F. H. Cao and J. Q. Zhang, *J. Electroanal. Chem*, 2005, **578**, 357–367.
12 X. Huang, Y. Chen, T. Fu, Z. Zhang and J. Zhang, *J. Electrochem. Soc.*, 2013, **160**, D530–D537.
13 E. Budevski, W. Obretenov, W. Bostanov, G. Staikov, J. Doneit, K. Jüttner and W. Lorenz, *Electrochim. Acta*, 1989, **34**, 1023 – 1029.
14 C. Gabrielli, F. Huet and M. Keddam, *Electrochim. Acta*, 1986, **31**, 1025–1039.
15 J. J. Kim, *Mater. Lett.*, 2007, **61**, 4000–4002.
16 R. Cottis, *Corrosion*, 2001, **57**, 265–285.
17 H. A. A. Al-Mazeedi and R. A. Cottis, *Electrochim. Acta*, 2004, **49**, 2787–2793.
18 U. Bertocci, J. Frydman, C. Gabrielli, F. Huet and M. Keddam, *J. Electrochem. Soc.*, 1998, **145**, 2780–2786.
19 F. Mansfeld and H. Xiao, *J. Electrochem. Soc.*, 1993, **140**, 2205–2209.
20 F. Mansfeld and Z. Sun, *Corrosion*, 1999, **55**, 915–918.
21 J. Smulko, K. Darowicki and A. Zieliński, *Electrochim. Acta*, 2002, **47**, 1297–1303.
22 K. Darowicki, A. Krakowiak and A. Zieliński, *Electrochem. Commun.*, 2002, **4**, 158–162.
23 P. Planinšič and A. Petek, *Discrete Wavelet Transforms - Biomedical Applications*, IntechOpen, Rijeka, 2011, ch. 11.
24 R. Moshrefi, M. G. Mahjani and M. Jafarian, *Electrochem. Commun.*, 2014, **48**, 49–51.
25 A. M. Homborg, E. P. M. Van Westing, T. Tinga, G. M. Ferrari, X. Zhang, J. H. W. De Wit and J. M. C. Mol, *Electrochim. Acta*, 2014, **116**, 355–365.
26 A. M. Homborg, R. A. Cottis and J. M. C. Mol, *Electrochim. Acta*, 2016, **222**, 627 – 640.
27 U. Bertocci, F. Huet, R. P. Nogueira and P. Rousseau, *Corrosion*, 2002, **54**, 337–347.

28 F. Mansfeld, Z. Sun, C. H. Hsu and A. Nagiub, *Corros. Sci.*, 2001, **43**, 341–352.

29 M. Jakubowska, *Electroanalysis*, 2011, **23**, 553–572.

30 A. M. Homborg, T. Tinga, X. Zhang, E. P. M. Van Westing, P. J. Oonincx, J. H. W. De Wit and J. M. C. Mol, *Electrochim. Acta*, 2012, **70**, 199–209.

31 B. M. Grafov, A. L. Klyuev and A. D. Davydov, *J. Solid State Electrochem.*, 2018, **22**, 1661–1667.

32 T. Claasen and W. Mecklenbrauker, *Philips J. Res.*, 1980, **35**, 217–250.

33 E. Wigner, *Phys. Rev.*, 1932, **40**, 749–759.

34 J. Ville, *Theorie et applications de la notion de signal analytique, Cables et Transmissions 2A (1948), 61–74. English translation by I. Selin, Theory and applications of the notion of complex signal*, Rand corporation technical report t-92 technical report, 1958.

35 B. Boashash and M. Mesbah, *Applications in Time-Frequency Signal Processing*, CRC Press, Boca Raton, 2003, pp. 339–369.

36 P. Flandrin, *Time-Frequency/Time-Scale Analysis*, Academic Press, 1999, vol. 10, pp. 183 – 307.

37 F. Auger and P. Flandrin, *IEEE Trans. Signal Process.*, 1995, **43**, 1068–1089.

38 M. J. Shensa, *IEEE Trans. Signal Process.*, 1992, **40**, 2464–2482.

39 A. Aballe, M. Bethencourt, F. Botana and M. Marcos, *Electrochim. Acta*, 1999, **44**, 4805–4816.

40 M. Shahidi, R. Farrehi Moghaddam, M. R. Gholamhosseinzadeh and S. M. A. Hosseini, *J. Electroanal. Chem*, 2013, **693**, 114–121.

41 J. Y. Huang, Y. B. Qiu and X. P. Guo, *Corros. Eng., Sci. Technol.*, 2010, **45**, 288–294.

42 B. Zhao, J. H. Li, R. G. Hu, R. G. Du and C. J. Lin, *Electrochim. Acta*, 2007, **52**, 3976–3984.

43 L. Cohen, *Proc. IEEE*, 1989, **77**, 941–981.

44 I. Zayed, *IEEE Signal Proc. Lett.*, 1998, **5**, 206–208.

45 B. Boashash and A. P. Reilly, *Time-frequency signal analysis*, Longman Cheshire, Melbourne, 1992, ch. 7, pp. 163–181.

46 B. Boashash, *Time-frequency signal analysis and processing: a comprehensive reference*, Academic Press, 2015.

47 F. Auger, P. Flandrin, P. Goncalves and O. Lemoine, *Time-Frequency Toolbox*, http://tftb.nongnu.org/, 1996.

48 C. Wang, Y. Cai, C. Ye, S. Dong, X. Cai, Y. Cao and C. Lin, *Electrochem. Commun.*, 2018, **90**, 11–15.

49 S. S. Jamali, Y. Zhao, Z. Gao, H. Li and A. C. Hee, *J. Ind. Eng. Chem.*, 2016, **43**, 36–43.

50 M. Palimi, E. Alibakhshi, G. Bahlakeh, B. Ramezanzadeh and M. Mahdavian, *J. Electrochem. Soc.*, 2017, **164**, C709–C716.

51 R.-W. Bosch, R. A. Cottis, K. Csecs, T. Dorsch, L. Dunbar, A. Heyn, F. Huet, O. Hyökyvirta, Z. Kerner, A. Kobzova, J. Macak, R. Novotny, J. Öijerholm, J. Piippo, R. Richner, S. Ritter, J. M. Sánchez-Amaya, A. Somogyi, S. Väisänen and W. Zhang, *Electrochim. Acta*, 2014, **120**, 379 – 389.

52 I. Jevremovic and A. Erbe, *Replication Data for: The Reassigned Pseudo Wigner-Ville Transform in Electrochemical Noise Analysis*, https://doi.org/10.18710/LUISQN, 2019.

53 R. Foley, *Corrosion*, 1986, **42**, 277–288.

54 R. Buchheit, *J. Electrochem. Soc.*, 1995, **142**, 3994–3996.

55 Z. Szklarska-Smialowska, *Corros. Sci.*, 1999, **41**, 1743–1767.

56 *Signal analysis and prediction*, ed. A. Prochazka, N. G. Kingsbury, P. J. W. Payner and J. Uhlir, Springer, New York, 1998.

57 M. Hashimoto, S. Miyajima and T. Murata, *Corros. Sci.*, 1992, **33**, 905 – 915.

58 U. Bertocci and J. Kruger, *Surf. Sci.*, 1980, **101**, 608–618.

59 K. Videm, 1974.

60 J. R. Davis, *Corrosion of aluminum and aluminum alloys*, Asm International, 1999.

61 G. Frankel, *J. Electrochem. Soc.*, 1998, **145**, 2186–2198.

62 L. Organ, J. R. Scully, A. S. Mikhailov and J. L. Hudson, *Electrochim. Acta*, 2005, **51**, 225–241.

63 N. Sato, *Electrochim. Acta*, 1971, **16**, 1683–1692.

64 R. Baboian, *Corrosion tests and standards: application and interpretation*, ASTM International, Materials Park, 2005.

65 H. Leth-Olsen, J. H. Nordlien and K. Nisancioglu, *Corros. Sci.*, 1998, **40**, 2051–2063.

66 L. Guan, Y. Zhou, H. Lin, B. Zhang, J. Wang, E.-H. Han and W. Ke, *Corros. Sci.*, 2015, **95**, 6–10.

67 S. Pride, J. Scully and J. Hudson, *J. Electrochem. Soc.*, 1994, **141**, 3028–3040.

68 H. S. Isaacs, C. Scheffey and R. Huang, *ECS Transactions*, 2008, **11**, 1–12.

69 N. Birbilis and R. Buchheit, *J. Electrochem. Soc.*, 2005, **152**, B140–B151.

70 C. Blanc, B. Lavelle and G. Mankowski, *Corros. Sci.*, 1997, **39**, 495–510.

71 H.-H. Strehblow and B. Titze, *Corros. Sci.*, 1977, **17**, 461–472.

72 D. Williams, C. Westcott and M. Fleischmann, *J. Electrochem. Soc.*, 1985, **132**, 1796–1804.

73 C. Punckt, M. Bölscher, H. H. Rotermund, A. S. Mikhailov, L. Organ, N. Budiansky, J. R. Scully and J. L. Hudson, *Science*, 2004, **305**, 1133–1136.

74 P. J. Denissen, A. M. Homborg and S. J. Garcia, *J. Electrochem. Soc.*, 2019, **166**, C3275–C3283.

75 G. Suresh and U. K. Mudali, *Corrosion*, 2013, **70**, 283–293.

76 C. Cai, Z. Zhang, F. Cao, Z. Gao, J. Zhang and C. Cao, *J. Electroanal. Chem.*, 2005, **578**, 143–150.